Inexpensive mount for a large millimeter-wavelength telescope

S. Padin

California Institute of Technology, 1200 East California Boulevard, Pasadena, California 91125, USA (spadin@caltech.edu)

Received 3 April 2014; revised 27 May 2014; accepted 30 May 2014;
posted 2 June 2014 (Doc. ID 209561); published 4 July 2014

A telescope mount with a single-point force support at the center of gravity of the primary mirror is proposed in order to eliminate much of the structure and cost of a large, millimeter-wavelength telescope. The single-point support gives repeatable thermal and gravitational deformation, so the surface of the primary can be controlled based on lookup tables for elevation and temperature. The new design is most appropriate for a survey telescope because locating the support above the vertex of the primary limits the range of motion of the mount to about 1 rad. A 30 m diameter, $\lambda = 850$ μm telescope with the proposed mount is a factor of 4 lighter than a design with a conventional elevation-over-azimuth mount, and roughly half the cost.

OCIS codes: (350.1260) Astronomical optics; (110.6770) Telescopes; (220.4880) Optomechanics.
http://dx.doi.org/10.1364/AO.53.004431

1. Introduction

The main cost drivers for a telescope are the accuracy of the mirrors, which is set by the wavelength, and the size of the telescope, which determines the mass of material in the structure [1]. Mirrors for short radio wavelengths are usually machined, e.g., from aluminum billet, or replicated, e.g., from carbon-fiber-reinforced plastic (CFRP), using well-developed technologies where a major cost reduction seems unlikely. The mass of the structure is typically an order of magnitude larger than the mass of the primary, and the cost of the structure is generally 1/3 to 1/2 of the total, so reducing mass is a particularly effective means of controlling cost. The choice of materials is also a cost driver, with a complicated trade-off between the cost of materials and the cost of the control systems that are needed to achieve the required pointing and surface errors. CFRP has four times the specific stiffness of steel [2], and a ten times lower coefficient of thermal expansion (CTE), so a completely passive CFRP structure is sometimes used instead of a steel structure with active surface control, despite as much as an order of magnitude higher cost for CFRP.

Telescopes for short radio wavelengths usually have a concave primary mirror supported by an elevation-over-azimuth mount. The arrangement is versatile, but expensive for a large telescope. If the telescope is intended mainly for survey work, the cost can be reduced by limiting the range of motion, so the mount is simpler and less massive. An example of this approach is the 6 m diameter, millimeter-wavelength Atacama Cosmology Telescope (ACT), with an elevation range of 30°–60° [3]. Telescopes with even more limited range of motion include the 10 m diameter, optical-wavelength Hobby Eberly Telescope (HET), which is fixed at 55° elevation but can drive over the full azimuth range [4], and the 1000 ft diameter, radio-wavelength Arecibo telescope, which has a completely fixed primary [5]. The telescope structure can also be simplified by minimizing the interface features that are typically used to connect the primary to the elevation axis of the mount, e.g., the Invar cone that supports the primary backup structure in the Atacama Large Millimeter Array antennas [6], or the large, hexagonal, dish-mounting platform in the Caltech Submillimeter Observatory (CSO) [7]. The elevation

1559-128X/14/204431-09$15.00/0

axis interface is challenging because an overconstrained connection causes thermal and gravitational deformation of the mount to spoil the surface of the primary, while a connection with low stiffness results in large pointing errors due to wind buffeting. Examples of telescopes with small primary support interfaces are the HET, which has a three-point kinematic connection [4], and the Array for Microwave Background Anisotropy (AMiBA), which has a Stewart platform [8].

In this work, these cost control approaches are applied to a large, millimeter-wavelength telescope on a small, inexpensive mount. The mount has 1 rad range of motion, which is reasonable for survey work. The telescope is 30 m in diameter, and it operates at $\lambda = 850$ μm. Thermal emission from cold dust in the earliest galaxies is bright in this band [9], and a diameter of 30 m gives enough angular resolution to solve the problem of identifying sources in images at other wavelengths [10]. High efficiency at $\lambda = 850$ μm requires <20 μm rms surface error (for >90% Strehl ratio) [11], which can be achieved with inexpensive machined panels [12]. The proposed design fills a gap in capability because existing large, single-dish telescopes are on poor sites and have low efficiency at short millimeter wavelengths [13–15].

A viable survey telescope requires the mirrors, the science instrument, and a means of pointing these components over a reasonable range. The goal here is to minimize everything else in the telescope, which leads to a design where the primary mirror is the main structure. This work therefore begins with a description of the primary mirror, followed by an explanation of the single-point force support scheme for the mount, an analysis of the telescope performance, and an estimate of the cost savings.

2. Inexpensive Mount

A. Optical Configuration

This work is concerned mainly with the design of the telescope mount, but the mount must accommodate a useful optical configuration. At millimeter wavelengths, two practical constraints drive the optical design:

1. Signals must be brought into a cold box that contains the detectors. A low-loss, millimeter-wavelength vacuum window cannot be larger than ~0.5 m diameter, so a wide-field instrument requires a segmented window, which must be mounted at a focus to minimize obscuration by the window support structure [16,17]. In an on-axis telescope, the Cassegrain or Gregory focus is the first easily accessible location for the window.

2. Detectors for large arrays generally have low directivity, so a cold stop must be provided to control the illumination of the telescope. Some relay optics are needed to generate a pupil for the stop. A simple relay with an intermediate pupil makes the final focus more concave when viewed from the sky, so it is easier to achieve a flat final focus if the relay input is the convex focus of a Gregory telescope [18]. When the field of view (FOV) is large, the telescope focus must be fast to keep the size of the relay optics reasonable. In this case, the instrument is close to the secondary, which is convenient for a mount with a single-point force support because there is a stiff structure above the primary vertex that can be used to support the instrument.

Figure 1 and Table 1 give details of the optical configuration for this work. The telescope is a Cassegrain design with a fast primary, chosen to keep the structure compact in order to reduce wind shake. A camera is mounted at the Cassegrain focus, between

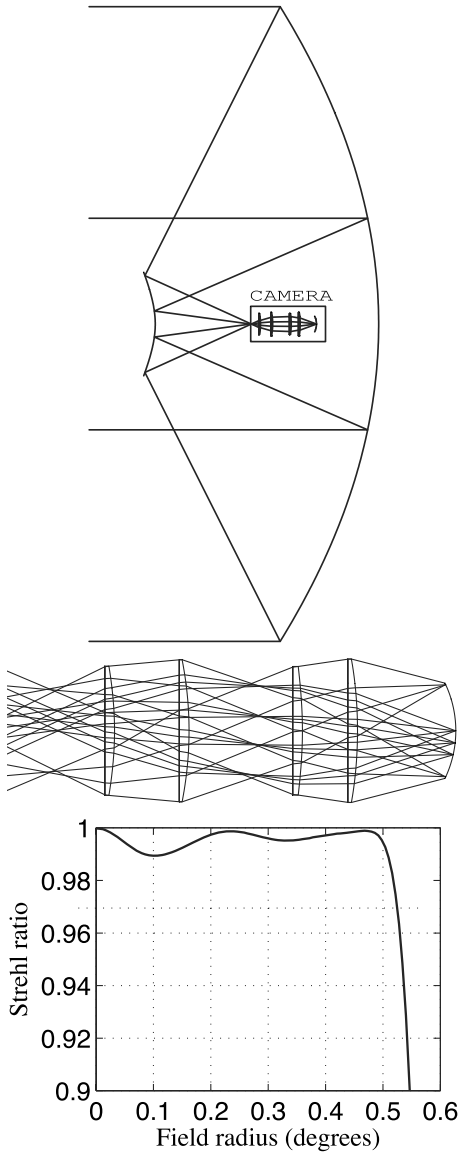

Fig. 1. Telescope layout (top), camera layout (center), and Strehl ratio versus field radius at $\lambda = 850$ μm (bottom). The camera window is at the Cassegrain focus, which is on the left in the camera layout. The camera has 2 alumina lenses to generate a pupil for the cold stop, and another 2 lenses to generate the final image. Each lens has one aspheric surface.

Table 1. Telescope Optical Prescription[a]

Parameter	Value	Units
Primary diameter	30	m
Primary focal ratio	0.4	
Primary conic constant	−1.071172	
Primary to secondary separation	10.56	m
Secondary radius of curvature	4.235	m
Secondary conic constant	−5.608707	
Secondary diameter	4.893	m
Secondary to image separation	4.5	m
Image focal ratio	1.25	
Image radius of curvature	1.6	m

[a]Image refers to the Cassegrain focus, not the camera focus. The primary and secondary are both more eccentric than for an aplanatic telescope.

the primary and secondary. The camera contains a relay with four alumina lenses [19,20] that generate a sharp pupil and reimage the Cassegrain focus at f/1.5 with >99% Strehl ratio over 1° FOV. The final focus is roughly telecentric in the sense that the beam is normal to the focal surface, but that surface is convex with 850 mm radius of curvature. A flat, telecentric final focus can be achieved with a Gregory design at the expense of a taller telescope structure. Many other optical configurations are possible, but Fig. 1 provides a reasonable basis for the mechanical design of the telescope.

B. Primary

The general configuration of the primary is machined aluminum panels on a steel, spaceframe truss, with active control of the piston, tip, and tilt of each panel based on lookup tables (or models) for elevation and truss temperature. A 30 m diameter, $\lambda = 850$ μm primary requires active control of gravitational deformation no matter what material is used for the truss. Expanding the scope of the control to include thermal deformation adds little to the cost of the control system, but allows the use of inexpensive materials, which helps to reduce the cost of the telescope. The truss is a spaceframe because spaceframe structures can be modeled easily and accurately. Machined panels have been used on many telescopes and they represent a conservative, relatively inexpensive approach. A surface error of ∼5 μm rms, including thermal and gravitational deformation, can be achieved on ∼1 m panels with an areal density of ∼10 kg m^{-2} [21].

The primary truss for a radio telescope is typically $D/4$ thick, where D is the primary diameter, so the surface error due to thermal deformation is $\epsilon \sim \mathrm{CTE} \times \Delta T \times D/4$, where ΔT is the temperature variation across the truss. During nighttime observations $\Delta T \sim 1$ K [22], but we can measure the temperature of the truss struts to ∼0.2 K, calculate the profile of the primary, and apply corrections. The surface error is then $\epsilon \sim \mathrm{CTE} \times D/20$. For >90% Strehl ratio, $\epsilon < \lambda/39$, so $D < \lambda/(1.95 \times \mathrm{CTE})$, i.e., $D(\text{in meters}) < 42\lambda(\text{in mm})$ for steel. A 30 m diameter, $\lambda = 850$ μm telescope with a steel truss should achieve good performance using active control based on strut temperature measurements, without the cost and complexity of a panel edge sensor system. Thermal deformation of the primary can be calculated using a finite element model, but the model must be optimized based on surface error measurements with different temperature distributions across the truss. Initial optimization could be just a simple adjustment of the overall CTE for the truss, but final optimization must also account for spatial variations in CTE. Control based on lookup tables for elevation and truss temperature requires repeatable structural deformations, so the joints in the truss must not slip. Good repeatability also favors a design with a kinematic support for the primary.

With 1 m diameter panels and three actuators per panel, there are ∼2000 actuators in the primary, so the actuators must be simple and reliable. Here, the panels are mounted kinematically, with a radial support consisting of a ball engaging a hole in the center of the back of the panel, a ball in a slot to constrain rotation, and three actuators that carry only axial loads. Each actuator has a simple stepper-motor-driven screw with a plain nut. An accurate home position switch is included at one end of the actuator range, so motor steps can be counted to monitor the position of the actuator. Counting steps is reasonable in this case because the actuator position error due to backlash, friction, and thermal deformation can be a few micrometers rms. The same approach probably would not work at short submillimeter wavelengths. Initial positions for the actuators can be obtained from measurements of the primary surface using a laser tracker, which will give ∼100 μm rms surface error on a 30 m diameter telescope [3]. Final alignment will require millimeter-wavelength holography measurements [23,24].

The basic tiling pattern for the primary panels is hexagonal, because this allows the truss to step from the panel scale to six support points in just a couple of layers. The truss has a thin, dense top layer in the form of hexagonal columns; a deep, sparse, second layer with tetrahedral cells; and a hexagonal pyramid for the third layer (see Figs. 2 and 3). The complete truss is a deep cone, similar to the homologous truss for the 100 m diameter Effelsberg Telescope [25], but the geometry follows the approach used for the CSO [7], with many struts running parallel to the optical axis of the primary. Truss nodes are simple extrusions with radial tabs, so interlayer connections run between tabs in the same plane.

C. Mount

The conventional approach for the mount is to support the primary on an elevation axis through the center of gravity (COG). Yoke or c-ring structures are typically used, but these add considerable mass and cost, and a counterweight is usually required [6,26,27]. Changing to a Stewart platform [28,29] eliminates much of the mount structure, but results

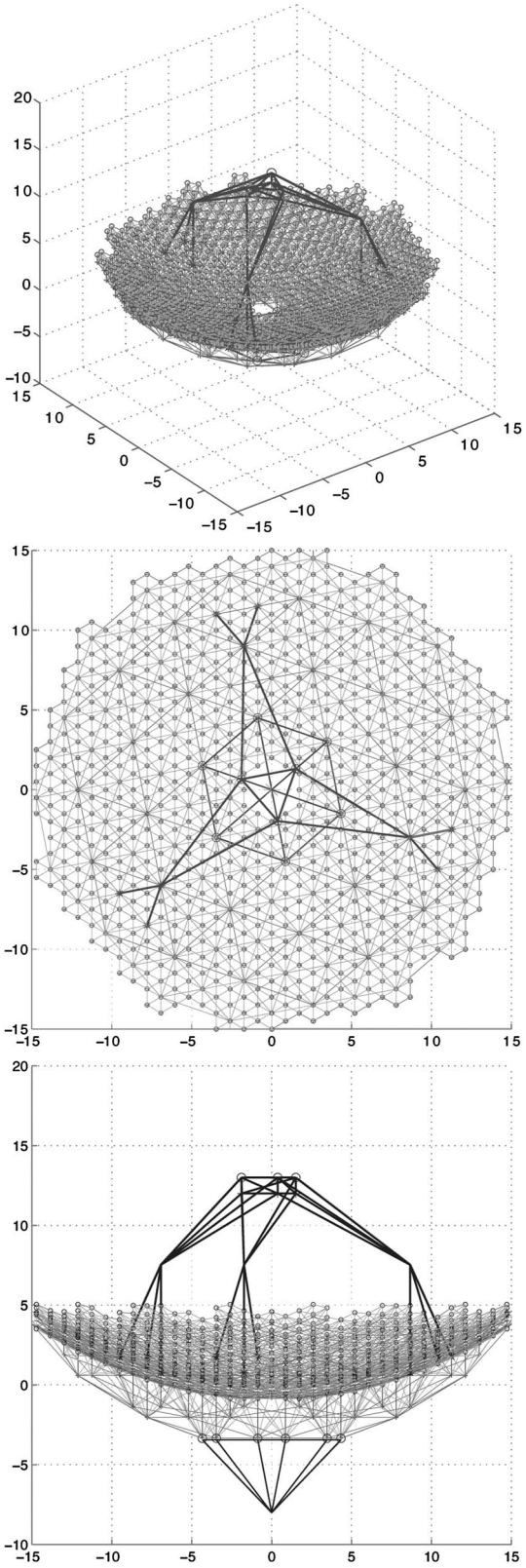

Fig. 2. Truss configuration. Dimensions are in meters.

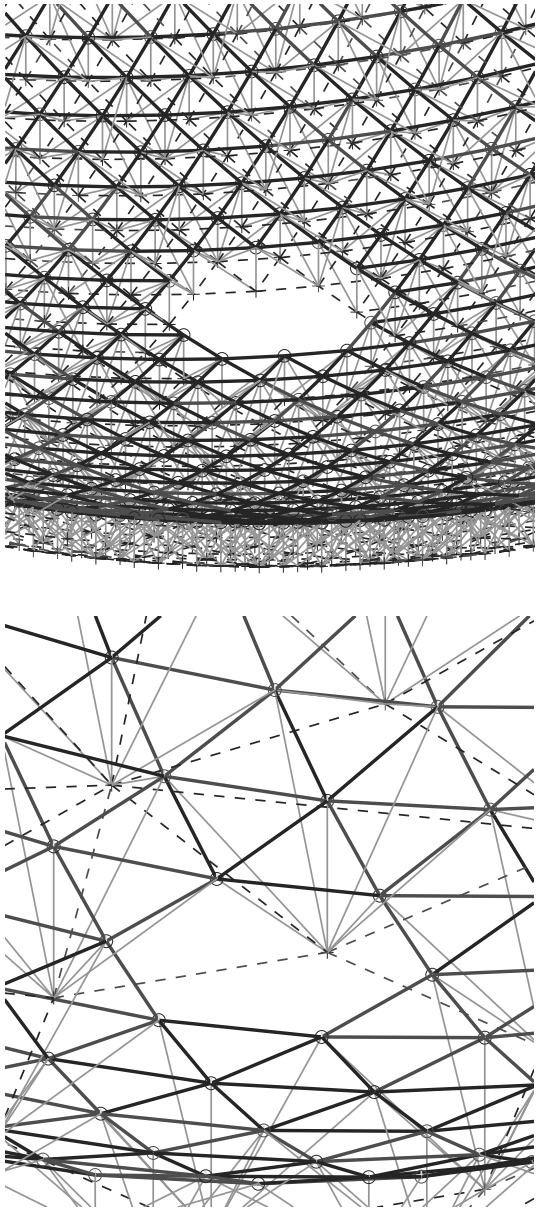

Fig. 3. Truss top and second layer details. Both views show the same part of the truss, at the same scale. Circles/crosses are nodes on the front/back of a layer and bold/dashed/light lines are struts on the front/back/inside. Each second-layer front node connects to the center of a hexagonal column in the top layer. The radial support at the center of each panel is attached to a top-layer front node. The panel actuators are mounted on a light frame (not shown) attached to the axial, top-layer strut behind the panel.

in an unbalanced configuration with large forces and moments on the jacks and joints, so any play or backlash causes large, nonrepeatable pointing errors [8]. The solution proposed here is to support the primary on a spherical rotary joint at the COG. With a single-point support at the COG, no force is required to position the primary, and deformations in the mount cannot be transferred to the primary, so thermal and gravitational deformation of the primary will be highly repeatable. The COG is accessible if the instrument is mounted between the primary and secondary and the conical tip of the truss is flipped over, so the apex of the cone is at the COG. The penalty for flipping the tip of the truss is a thinner structure that has lower stiffness.

If the spherical rotary joint is fixed, it constrains the (x,y,z) position of the apex of the cone, leaving three free rotations: elevation and cross-elevation pointing, and rotation about the optical axis (parallactic angle). Connecting three jacks from the back of the truss to the ground is sufficient to fully constrain rigid-body motion of the primary, but the structure has low natural frequency and poor pointing performance in the wind. The stiffness can be improved by combining the spherical rotary joint with a Stewart platform, but to avoid overconstraining the structure, the spherical rotary joint must be mounted on a force support with no position constraints (see Fig. 4). In this configuration, the spherical rotary joint carries the weight of the primary and the Stewart platform sets the position. The mount is then much like the hard point and flotation supports used for large optical mirrors [30,31]. The platform jacks are counterweighted so they exert no force on the primary, and the spherical rotary joint is mounted on three hydraulic cylinders that are controlled to give zero force on the jacks due to the weight of the primary. The forces on the jacks are measured using load cells. In this configuration, the only forces at the jack connection points are due to wind and seismic loading. The jacks still have to be stiff to resist the wind, but they carry only small loads, so the jack nuts and joint bearings can be preloaded to eliminate backlash and play.

The range of motion of the mount is limited by interference between the truss and the support structure for the spherical rotary joint. The design in Fig. 4 has 1 rad of motion in elevation and cross elevation. The maximum change in jack length is a factor of 2 (3.84–7.86 m), so a single-stage telescoping design can be used. A larger change in jack length would require more space below the ground end of the jacks, leading to a complicated, expensive pier.

The platform jacks have servo loops, with encoders to measure jack length and speed, but pitch errors and thermal deformation of the jack screws cause large pointing errors [8], so the main pointing reference is a small optical telescope mounted on the truss. Offset optical pointing is straightforward at the 1″ level, i.e., 1/7th of the beamwidth for a 30 m telescope at $\lambda = 850$ μm, but extremely difficult at the 0.1″ level because of differential deflection between the main and guide telescopes [32].

D. Performance

A finite element model of the telescope in Fig. 4 was generated in MATLAB [33], then analyzed using ANSYS [34]. The model contains only beams, point masses, loads, and constraints, as shown in Table 2. The panels, truss strut connections, secondary, and instrument are represented by point masses located at truss nodes. All of the structure is made of A36 steel, except for the secondary support, which is a braced CFRP hexapod similar in configuration to the secondary support in the Giant Magellan Telescope [35,36]. Materials properties for the model

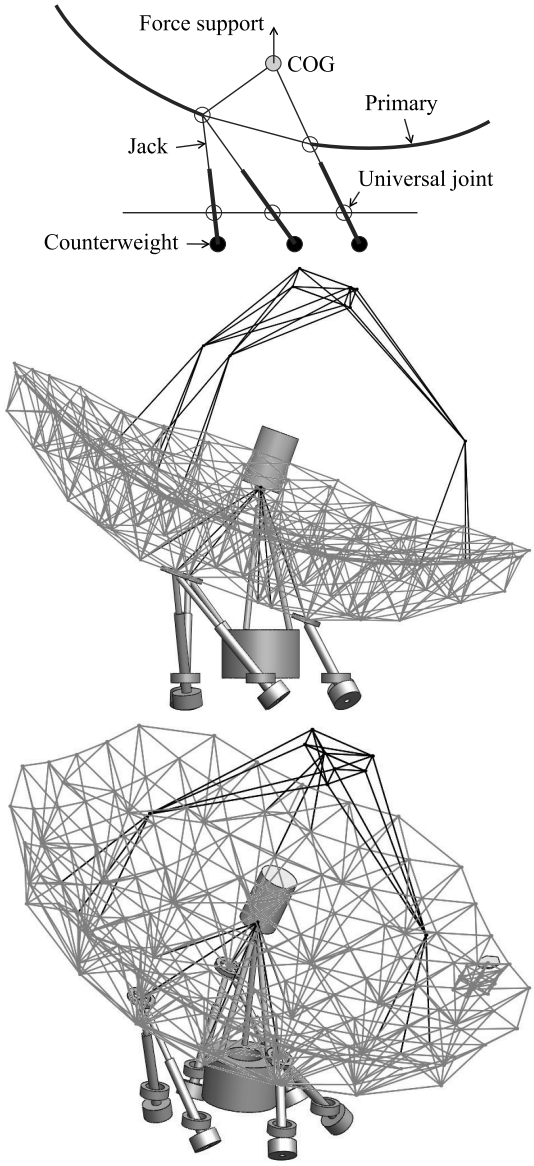

Fig. 4. General configuration (top) and design details (center and bottom) of a telescope with a single-point force support at the COG of the primary. The center picture shows only the second layer of the truss, but a single hexagonal panel and a small section of the top layer of the truss can be seen on the right of the bottom picture. The force support is at the top of the central tripod in the center and bottom pictures, and the cylindrical can immediately above the force support is the instrument package. Ground level is at the base of the annular pier that supports the tripod. The mount jacks have counterweights on the ground end. The rings above the counterweights, and at the tops of the jacks, represent universal joints.

are given in Table 3. The total mass of the telescope is 195 t (see Table 4), which is a factor ~4 smaller than existing 30 m designs [37,38].

Gravitational deformation is 0.88(1.71) mm p–p at 90°(65°) elevation, so the panel actuators must have a stroke of a few millimeters (see Fig. 5). The natural frequency of the primary with the three jack connection points fixed is 4.7 Hz (side-to-side sway), and the natural frequency of the complete telescope is 3.9 (3.2) Hz at 90°(65°) elevation (again, a side-to-side

Table 2. Finite Element Model Details

Component	Description	Material
Panel	30 kg point mass at each truss surface node (1 m^2 panel at 10 kgm^{-2} + 3 × 1.5 kg actuators + 10 kg actuator frame + 5 kg hardware)	
Truss top layer	25 mm OD × 2 mm wall, 1 kg point mass at each node	Steel
Truss 2nd layer	100 mm OD × 10 mm wall, 20 kg point mass at each node	Steel
Truss 3rd layer	300 mm OD × 25 mm wall, 160 kg point mass at each node	Steel
Secondary	1/3 t point mass at three top-end nodes, 1 t total (25 m^2 tiles at 10 kgm^{-2} + 400 kg subframe + 300 kg hexapod + 50 kg hardware)	
Secondary support	150 mm OD × 7.5 mm wall	CFRP
Instrument	3 t point mass 1.5 m above force support	
Jack	300 mm OD × 100 mm ID	Steel
Universal joint	1 t point mass at each end of jack	
Force support	1028 kN vertical at primary COG	
Fixed support	Ground end of universal joint at bottom of jack	
10 ms^{-1} wind	50 N at each truss surface node + 500 N at each of three top-end nodes	

Table 3. Materials Properties

Property	Units	Steel	CFRP
Density	$kg\,m^{-3}$	7850	1550
Young's modulus	GPa	210	290
CTE	$ppm\,K^{-1}$	12	−1
Poisson's ratio		0.3	0.3

Table 4. Telescope Mass

Component	Mass (t)
Panels and actuators	25
Truss	76
Secondary	1
Instrument	3
Jacks	15
Universal joints	12
Jack counterweights	63
Total	195

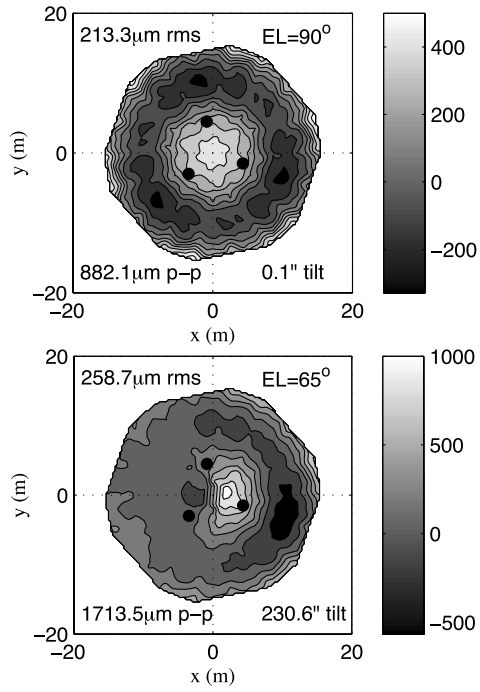

Fig. 5. Gravitational deformation, after correcting pointing and focus, at zenith (top) and elevation 65° toward +ve x (bottom). The gray scale is in micrometers. Black dots indicate the jack connection points on the back of the truss.

sway). With ∼4 Hz natural frequency, the mount servo should achieve a closed-loop bandwidth of ∼1 Hz. Practical steel antenna structures achieve a natural frequency (in Hz) of roughly $20 \times D^{-0.7}$ (D in meters) [39], i.e., ∼2 Hz for $D = 30$ m, so the design of Fig. 4 compares well with existing structures. Increasing the diameter of the jack screws does not improve the natural frequency of the telescope much because the mass of the jacks and associated counterweights also increases. The stiffness of the jacks ranges from 1.6 to 3.3 $kN\,\mu m^{-1}$ (depending on extension), which is a few times larger than for the jacks in the Stewart platform in the 6 m diameter AMiBA telescope [8].

Deformation due to wind forces is a serious concern because removing material to reduce cost results in a light structure that deforms easily in the wind. The pointing error due to wind torque T is roughly $T/(I\omega_0^2)$ rad, where I is the moment of inertia and ω_0 is the natural frequency, and since inertia scales roughly with mass and cost, the pointing error due to wind scales roughly as 1/cost. Placing the telescope inside an enclosure would shield it from the wind and protect it from severe weather, but even a simple enclosure would be prohibitively expensive. The only option seems to be active control of wind-induced deformations, which is common for optical telescopes but has not been demonstrated on a radio telescope. For the telescope in Fig. 4, 10 ms^{-1} wind, which is a typical 90th percentile nighttime wind speed at a good millimeter-wavelength observing site [40], causes 38(63)″ pointing error and 102(71) μm rms surface error at 90°(65°) elevation (see Fig. 6), so active control must improve wind-induced deformations by an order of magnitude. The timescale for corrections is the wind crossing time for the primary,

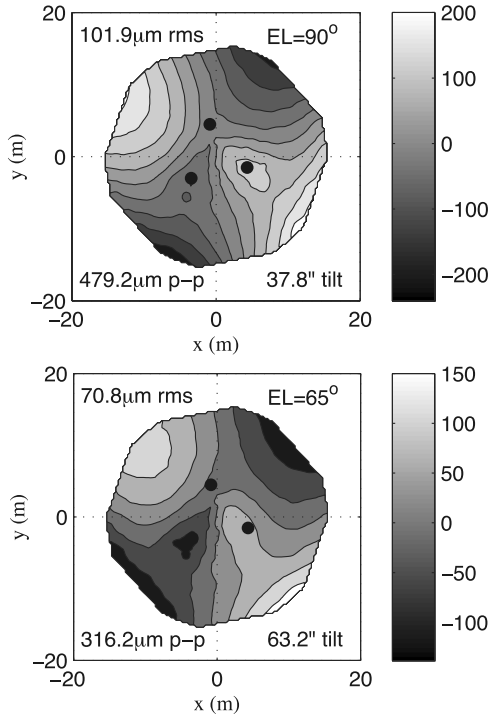

Fig. 6. Wind-induced deformation, after correcting pointing and focus, at zenith (top) and elevation 65° toward +ve x (bottom) due to a 10 ms^{-1} wind blowing along the x axis. The gray scale is in micrometers. Black dots indicate the jack connection points on the back of the truss.

which is ~3 s for a 30 m diameter telescope in a 10 ms^{-1} wind. Offset guiding with a small optical telescope can be used to correct the pointing, but this is not straightforward for millimeter-wavelength imaging observations because the telescope must scan at ~1° s^{-1} to freeze atmospheric brightness fluctuations, so the pointing camera readout rate must be ~1 kHz to give <1″ rms image smearing. At 1 kHz readout rate, a 0.3 m diameter pointing telescope with ~1° FOV is needed to ensure that a guide star is always visible at night (see Appendix A). It is impractical to measure the surface profile of the primary during a scan, so the primary must be controlled based on measurements of the wind pressure and a stiffness model. A wind speed of 10 ms^{-1} corresponds to ~50 Pa at the primary, so equipping the panels with pressure sensors that have an accuracy of ~5 Pa will allow an order of magnitude improvement in wind-induced deformations. The additional equipment for active control of wind effects is just a small optical telescope and pressure sensors on the panels, so the cost is low, but testing the pointing and surface control systems will be challenging.

E. Strength

Low cost demands a light, exposed telescope, but the structure must be strong enough to survive high winds. The wind speed on a high-altitude site might be as much as 70 ms^{-1}, in which case the peak stress due to wind forces in the design of Fig. 4 is 182 (200) MPa at 90°(65°) elevation, with the highest stresses in the cone and the layer 2 truss struts that connect to it. Under gravity loading, the peak stress is 23.2(39.6) MPa at 90°(65°) elevation, with the highest stresses again in the cone and associated layer 2 struts. The total stress due to the combination of survival wind forces and gravity is 240 MPa, which is just below the 250 MPa yield strength of A36 steel, so the structure cannot be made much lighter (see Appendix B). During a severe earthquake, the seismic acceleration in the structure might be 4–5 times the acceleration due to gravity, in which case the peak stress due to the combination of gravity and seismic loading is again 240 MPa. The stresses calculated here demonstrate that the structure will not yield under survival conditions at a typical millimeter-wavelength observing site, so the telescope will not collapse. However, the strength of the structure may have to be adjusted to account for site-specific environmental conditions and building codes.

Table 5. Cost Estimates for a 30 m Diameter, $\lambda = 850$ μm Telescope

Subsystem	Cost $M	Component	Cost $M	Basis
Primary	11.1			
		Panels	7.0	700 m^2 machined aluminum at \$10 k/m^2
		Actuators	1.1	2100 (3 per panel) at \$500 each
		Truss	1.5	76 t steel at \$20/kg
		Secondary support	0.5	1 t CFRP at \$200/kg + \$300 k for hexapod
		Secondary mirror	1.0	Machined aluminum panels on CFRP subframe
EL-over-AZ mount	17.4			
		Steel structure	14	700 t steel at \$20/kg
		Drives and bearings	2.5	3 bearings at \$500 k each + 2 drives at \$500 k each
		Pier	0.9	300 m^3 concrete at \$3 k/m^3
New mount	4.1			
		Jacks and drives	0.6	6 at \$100 k each
		Jack counterweights	1.3	63 t steel at \$20/kg
		Universal joints	1.2	12 at \$100 k each
		Spherical rotary joint	0.5	\$250 k joint + 3 hydraulic cylinders at \$50 k each
		Pier	0.5	150 m^3 concrete at \$3 k/m^3
Design	2.0			10 person-years, same for new and EL-over-AZ mounts

3. Conclusion

A new telescope mount is proposed with a single-point force support to carry the weight of the primary and a Stewart platform to set the position. The key advantage of the design is the small size of the mount, which results in roughly a factor 2 cost savings for a 30 m diameter, $\lambda = 850$ μm telescope (see Table 5). The platform exerts no force on the primary, except to resist wind and seismic loading, so thermal and gravitational deformation of the primary is highly repeatable, which allows corrections based on lookup tables for elevation and temperature. The main disadvantage of the new mount is that the range of motion is limited to about 1 rad, but this is enough for a telescope that will work mainly on surveys.

Appendix A: Optical Pointing

This appendix demonstrates that optical pointing while scanning at $1°\ s^{-1}$ is viable with a ~0.5 m-diameter pointing telescope. At $\lambda \sim 1$ μm, the integrated source density up to magnitude m at high galactic latitude is [41]

$$\rho(<m) \approx 10 \times (\lambda \text{ in } \mu\text{m}) \times 10^{(m-10)/3.1} \text{ deg}^{-2}, \quad \text{(A1)}$$

where

$$m = -2.5 \log(f/f_0), \quad \text{(A2)}$$

with f being the source flux density, and $f_0 \approx 2000 \text{ Jy} \times 1/\lambda \text{ (in } \mu\text{m)}$ the flux density at $m = 0$ [42]. Thus, the number of sources brighter than f in solid angle Ω (in sr) is

$$N(>f) \approx 20\Omega \times (\lambda \text{ in } \mu\text{m}) \times (f/f_0)^{-4/5}. \quad \text{(A3)}$$

If there are at least a few pixels across the point spread function (PSF), the centroid can be measured with accuracy

$$\sigma \approx \frac{\text{FWHM}}{\text{SNR}}, \quad \text{(A4)}$$

where FWHM $\approx 1.2\lambda/d$ is the full width at half maximum of the PSF, d is the pointing telescope aperture diameter, and SNR is the signal-to-noise ratio. For a nighttime observation with a fast read-out rate, the SNR is limited by detector read noise, so

$$\text{SNR} = \frac{f d^2 R \tau}{r n^{1/2}}, \quad \text{(A5)}$$

where R is the response of a system with unit aperture diameter (e.g., in electrons $\text{s}^{-1}\,\text{mJy}^{-1}$), τ is the integration time, n is the number of pixels used to calculate the centroid, and r is the read noise (e.g., in electrons). R (in electrons $\text{s}^{-1}\,\text{mJy}^{-1}$) $\approx 10^{-29}\Delta\nu\eta/(h\nu)$, where ν is the frequency, $\Delta\nu$ is the bandwidth, η is the efficiency of the system, and h is Planck's constant. The fractional bandwidth is typically 20% for bands in the $\lambda = 0.5$ to 2 μm range, and an efficiency of 1/4 is reasonable, so $R \approx 750$ electrons $\text{s}^{-1}\,\text{mJy}^{-1}$.

Combining Eqs. A1–A5 gives

$$N \approx (\Omega/1 \text{ deg}^2)(\lambda/1 \text{ μm})^{-3/5}(\sigma/1'')^{4/5}(d/0.17 \text{ m})^{12/5} \times (\tau/1 \text{ ms})^{4/5}(r/15 \text{ electrons})^{-4/5}(n/9)^{-2/5}, \quad \text{(A6)}$$

where the default values reflect the goal of measuring the pointing within 1″ rms (1/7th of the beam-width of a 30 m, $\lambda = 850$ μm telescope) at a scan speed of $1°\ \text{s}^{-1}$ (3″ image motion in 1 ms). For $N = 5$, which will ensure that a few sources are always visible, the telescope must have $d = 0.32$ m and 1° FOV, or $d = 1$ m and 1/4° FOV.

Appendix B: Wind Loading

This appendix gives an estimate of the minimum mass of a truss that can survive wind loading. Each quadrant of the truss is modeled as a radial beam, fixed at the center of the primary. The beam is $D/2$ long (the radius of the truss), $D/20$ wide at the fixed end (roughly the radius of the hole in the center of the primary), and $D/4$ thick (the thickness of the truss), and the area for wind loading is $A = \pi(D/2)^2/4$. The maximum stress in the beam is [43]

$$s \sim AP(D/2)/(Z) \sim 200P/\zeta, \quad \text{(B1)}$$

where P is the wind pressure, $Z = \zeta(D/20)(D/4)^2/6$ is the section modulus, and ζ is the truss filling factor, which is typically 0.1%. The mass of the truss is

$$M = \pi(D/2)^2(D/4)\rho\zeta, \quad \text{(B2)}$$

where ρ is the density of the truss material. Combining Eqs. (B1) and (B2) gives

$$M \sim 40PD^3\rho/s. \quad \text{(B3)}$$

If the survival wind speed is 70 ms^{-1} ($P = 2450$ Pa), a 30 m diameter truss made of A36 steel ($\rho = 7850\ \text{kgm}^{-3}$ and 250 MPa yield strength) must have a mass of ~83,000 kg, which is similar to the mass of the truss in Table 4.

This work was supported by the John B. and Nelly Kilroy Foundation.

References

1. S. von Hoerner, "Design of large steerable antennas," Astron. J. **72**, 35–47 (1967).
2. E. J. Barbero, *Introduction to Composite Materials Design*, 2nd ed. (CRC Press, 2011), Chap. 1.
3. A. D. Hincks, P. A. R. Ade, C. Allen, M. Amiri, J. W. Appel, E. S. Battistelli, B. Burger, J. A. Chervenak, A. J. Dahlen, S. Denny, M. J. Devlin, S. R. Dicker, W. B. Doriese, R. Dunner, T. Essinger-Hileman, R. P. Fisher, J. W. Fowler, M. Halpern, P. C. Hargrave, M. Hasselfield, G. C. Hilton, K. D. Irwin, N. Jarosik, M. Kaul, J. Klein, J. M. Lau, M. Limon, R. H. Lupton, T. A. Marriage, K. L. Martocci, P. Mauskopf, S. H. Moseley, C. B. Netterfield, M. D. Niemack, M. R. Nolta, L. Page, L. P. Parker, A. J. Sederberg, S. T. Staggs, O. R. Stryzak, D. S.

Swetz, E. R. Switzer, R. J. Thornton, C. Tucker, E. J. Wollack, and Y. Zhao, "The effects of the mechanical performance and alignment of the Atacama Cosmology Telescope on the sensitivity of microwave observations," Proc. SPIE **7020**, 70201P (2008).
4. V. L. Krabbendam, T. A. Sebring, F. B. Ray, and J. R. Fowler, "Development and performance of Hobby Eberly Telescope 11 meter segmented mirror," Proc. SPIE **3352**, 436–445 (1998).
5. J. W. Findlay, "Radio telescopes," IEEE Trans. Antennas Propag. **12**, 853–864 (1964).
6. J. W. M. Baars, *The Paraboloidal Reflector Antenna in Radio Astronomy and Communication* (Springer, 2007), Chap. 7.
7. R. B. Leighton, "A 10-meter telescope for millimeter and submillimeter astronomy," Final Technical Report for NSF Grant AST 73-04908 (California Institute of Technology, 1978).
8. P. M. Koch, M. Kesteven, H. Nishioka, H. Jiang, K.-Y. Lin, K. Umetsu, Y.-D. Huang, P. Raffin, K.-J. Chen, F. Ibanez-Romano, G. Chereau, C.-W. L. Huang, M.-T. Chen, P. T. P. Ho, K. Pausch, K. Willmeroth, P. Altamirano, C.-H. Chang, S.-H. Chang, S.-W. Chang, C.-C. Han, D. Kubo, C.-T. Li, Y.-W. Liao, G.-C. Liu, P. Martin-Cocher, P. Oshiro, F.-C. Wang, T.-S. Wei, J.-H. P. Wu, M. Birkinshaw, T. Chiueh, K. Lancaster, K.-Y. Lo, R. N. Martin, S. M. Molnar, F. Patt, and B. Romeo, "The AMiBA hexapod telescope mount," Astrophys. J. **694**, 1670–1684 (2009).
9. G. Lagache, J.-L. Puget, and H. Dole, "Dusty infrared galaxies: sources of the cosmic infrared background," Annu. Rev. Astron. Astrophys. **43**, 727–768 (2005).
10. R. J. Ivison, T. R. Greve, I. Smail, J. S. Dunlop, N. D. Roche, S. E. Scott, M. J. Page, J. A. Stevens, O. Almaini, A. W. Blain, C. J. Willott, M. J. Fox, D. G. Gilbank, S. Serjeant, and D. H. Hughes, "Deep radio imaging of the SCUBA 8-mJy survey fields: submillimetre source identifications and redshift distribution," Mon. Not. R. Astron. Soc. **337**, 1–25 (2002).
11. J. Ruze, "Antenna tolerance theory—a review," Proc. IEEE **54**, 633–640 (1966).
12. J. G. Mangum, J. W. M. Baars, A. Greve, R. Lucas, R. C. Snel, P. Wallace, and M. Holdaway, "Evaluation of the ALMA prototype antennas," Publ. Astron. Soc. Pac. **118**, 1257–1301 (2006).
13. F. P. Schloerb, "The large millimeter telescope," Proc. SPIE **7012**, 70120S (2008).
14. J. W. M. Baars, A. Greve, H. Hein, D. Morris, J. Penalver, and C. Thum, "Design parameters and measured performance of the IRAM 30-m millimeter radio telescope," Proc. IEEE **82**, 687–696 (1994).
15. D. Morris, M. Bremer, G. Butin, M. Carter, A. Greve, J. W. Lamb, B. Lazareff, J. Lopez-Perez, F. Mattiocco, J. Penalver, and C. Thum, "Surface adjustment of the IRAM 30 m radio telescope," IET Microwaves Antennas Propag. **3**, 99–108 (2009).
16. J. W. Fowler, M. D. Niemack, S. R. Dicker, A. M. Aboobaker, P. A. R. Ade, E. S. Battistelli, M. J. Devlin, R. P. Fisher, M. Halpern, P. C. Hargrave, A. D. Hincks, M. Kaul, J. Klein, J. M. Lau, M. Limon, T. A. Marriage, P. D. Mauskopf, L. Page, S. T. Staggs, D. S. Swetz, E. R. Switzer, R. J. Thornton, and C. E. Tucker, "Optical design of the Atacama Cosmology Telescope and the Millimeter Bolometric Array Camera," Appl. Opt. **46**, 3444–3454 (2007).
17. S. Padin, M. Hollister, S. Radford, J. Sayers, D. Woody, J. Zmuidzinas, G. Cortes-Medellin, T. Sebring, and G. Stacey, "CCAT optics," Proc. SPIE **7733**, 77334Y (2010).
18. D. J. Schroeder, *Astronomical Optics*, 2nd ed. (Academic, 2000), Chap. 9.
19. J. W. Lamb, "Miscellaneous data on materials for millimetre and submillimetre optics," Int. J. Infrared Millim. Waves **17**, 1997–2034 (1996).
20. Y. Inoue, T. Matsumura, M. Hazumi, A. T. Lee, T. Okamura, A. Suzuki, T. Tomaru, and H. Yamaguchi, "Cryogenic infrared filter made of alumina for use at millimeter wavelength," Appl. Opt. **53**, 1727–1733 (2014).
21. D. Woody, D. MacDonald, M. Bradford, R. Chamberlin, M. Dragovan, P. Goldsmith, J. Lamb, S. Radford, and J. Zmuidzinas, "Panel options for large precision radio telescopes," Proc. SPIE **7018**, 70180T (2008).
22. A. Greve and M. Bremer, *Thermal Design and Thermal Behaviour of Radio Telescopes and their Enclosures* (Springer, 2010), Chap. 9.
23. J. C. Bennett, A. P. Anderson, P. A. McInnes, and A. J. T. Whittaker, "Microwave holographic metrology of large reflector antennas," IEEE Trans. Antennas Propag. **24**, 295–303 (1976).
24. P. F. Scott and M. Ryle, "A rapid method for measuring the figure of a radio telescope reflector," Mon. Not. R. Astron. Soc. **178**, 539–545 (1977).
25. O. Hachenberg, B. H. Grahl, and R. Wielebinski, "The 100-meter radio telescope at Effelsberg," Proc. IEEE **61**, 1288–1295 (1973).
26. J. D. Kraus, *Radio Astronomy* (McGraw-Hill, 1966), Chap. 6.
27. W. N. Christiansen and J. A. Hogbom, *Radiotelescopes* (Cambridge, 1969), Chap. 3.
28. V. E. Gough, "Contribution to discussion of papers on research in automobile stability, control and tyre performance," Proc. Inst. Mech. Eng. Auto. Div. **171**, 392–394 (1956).
29. D. A. Stewart, "A platform with six degrees of freedom," Proc. Inst. Mech. Eng. **180**, 371–386 (1965).
30. J. DeVries, D. Neill, and E. Hileman, "LSST telescope primary/tertiary mirror hardpoints," Proc. SPIE **7739**, 77391J (2010).
31. C. Hull, S. Gunnels, M. Johns, J. Kern, A. Talmor, M. Ward, and S. Shectman, "Giant Magellan telescope primary mirror cells," Proc. SPIE **7733**, 773327 (2010).
32. S. Assawaworrarit and S. Padin, "An optical pointing telescope for radio astronomy," Publ. Astron. Soc. Pac. **124**, 242–246 (2012).
33. MathWorks, 3 Apple Hill Drive, Natick, Massachusetts 01760, USA.
34. ANSYS Inc., 275 Technology Drive, Canonsburg, Pennsylvania 15317, USA.
35. S. Gunnels, W. Davison, B. Cuerden, and E. Hertz, "The Giant Magellan Telescope (GMT) structure," Proc. SPIE **5495**, 168–179 (2004).
36. D. P. Woody, S. Padin, and T. Sebring, "CFRP truss for the CCAT 25 m diameter submillimeter-wave telescope," Proc. SPIE **7733**, 77332B (2010).
37. J. W. M. Baars, B. G. Hooghoudt, P. G. Mezger, and M. J. de Jonge, "The IRAM 30-m millimeter radio telescope on Pico Veleta, Spain," Astron. Astrophys. **175**, 319–326 (1987).
38. D. Woody, S. Padin, E. Chauvin, B. Clavel, G. Cortes, A. Kissil, J. Lou, P. Rasmussen, D. Redding, and J. Zolkower, "The CCAT 25 m diameter submillimeter-wave telescope," Proc. SPIE **8444**, 84442M (2012).
39. W. Gawronski, *Modeling and Control of Antennas and Telescopes* (Springer, 2008), p. 43.
40. J. P. P. Beaupuits, A. Otarola, F. T. Rantakyro, R. C. Rivera, S. J. E. Radford, and L.-A. Nyman, "Analysis of wind data gathered at Chajnantor," *ALMA Memo 497, National Radio Astronomy Observatory*, May 2004.
41. M. F. Skrutskie, R. M. Cutri, R. Stiening, M. D. Weinberg, S. Schneider, J. M. Carpenter, C. Beichman, R. Capps, T. Chester, J. Elias, J. Huchra, J. Liebert, C. Lonsdale, D. G. Monet, S. Price, P. Seitzer, T. Jarrett, J. D. Kirkpatrick, J. E. Gizis, E. Howard, T. Evans, J. Fowler, L. Fullmer, R. Hurt, R. Light, E. L. Kopan, K. A. Marsh, H. L. McCallon, R. Tam, S. Van Dyk, and S. Wheelock, "The two micron all sky survey (2MASS)," Astron. J. **131**, 1163–1183 (2006).
42. M. S. Bessel, "UBVRI photometry II: the Cousins VRI System, its temperature and absolute flux calibration, and relevance for two-dimensional photometry," Publ. Astron. Soc. Pac. **91**, 589–607 (1979).
43. E. Oberg, F. D. Jones, H. L. Horton, and H. H. Ryffel, *Machinery's Handbook*, 24th ed. (Industrial, 1992), p. 225.